Geophysical Research Letters

RESEARCH LETTER
10.1029/2020GL089985

Key Points:
- We introduce a method to find statistically significant transitions between the quantile states of stationary time series
- We reveal forecasting windows at intraseasonal time scales for tercile and quartile states of the South American rainfall Dipole index
- We report two robust and reliable time windows at 5 to 15 and 60 to 70 days, where we can forecast SAD states with 99% confidence

Supporting Information:
- Supporting Information S1

Correspondence to:
N. Díaz,
nicolasdiaznegrin@gmail.com

Citation:
Díaz, N., Barreiro, M., & Rubido, N. (2020). Intraseasonal predictions for the South American rainfall dipole. *Geophysical Research Letters*, *47*, e2020GL089985. https://doi.org/10.1029/2020GL089985

Received 24 JUL 2020
Accepted 20 OCT 2020
Accepted article online 29 OCT 2020

Intraseasonal Predictions for the South American Rainfall Dipole

Nicolás Díaz[1], Marcelo Barreiro[1], and Nicolás Rubido[1,2,3]

[1]Instituto de Física de Facultad de Ciencias, Universidad de la República, Montevideo, Uruguay, [2]Aberdeen Biomedical Imaging Centre, University of Aberdeen, Aberdeen, UK, [3]Institute for Complex Systems and Mathematical Biology, University of Aberdeen, Aberdeen, United Kingdom

Abstract The South American rainfall Dipole (SAD) is a renowned spatial structure present in the austral summer as part of the South American monsoon system. SAD phases have been related with extreme precipitations and severe droughts across South America, but are yet to be predicted. Here, we reveal two robust and reliable intraseasonal windows in the accumulated SAD index where we can forecast its quantile-state between 5 to 15 and 60 to 70 days in advance (99% significance level). These windows are insensitive to variations in the pole's size and accumulation window, and results are consistent across different quantiles states (median, tercile, and quartile). Our method, which is based on analyzing the lagged mutual information between future and present states, could be used in the development of early warnings for extreme rainfall events. Moreover, it is unrestricted to the present analysis, being applicable to other stationary signals where a forecast is missing.

Plain Language Summary The South American Dipole (SAD) is a spatially-extended rainfall system present in the austral summer. Its dipole behaviour means that it is composed of two regions (or poles): when one regions shows an increase in precipitation the other region shows a decrease in precipitation, and vice versa. Forecasting future SAD behaviour is particularly important as its extreme states have been associated with floods or droughts over these regions (which include highly populated areas, such as São Paulo, Brazil). Here, we introduce a method to predict the dipole's future state from statistical and information theory analyses. Our main results show that there are two time windows where forecasting future SAD states is possible: from 5 to 15 days and from 60 to 70 days. These windows belong to the intraseasonal time scale (from 10 to 90 days), which is a generally challenging time scale to have predictions and where forecasts are scarce.

1. Introduction

South America (SA) has a broad range of climate behaviors (Cavalcanti et al., 2016; Garreaud & Aceituno, 2007), both in space and time. This stems from its latitudinal extension that covers from equatorial to midlatitudes, its topography and heterogeneous vegetation, as well as its dependence on multiple modes of climate variability. Among the latter phenomena, we can highlight SA's climate dependence on El Niño–Southern Oscillation (ENSO) at interannual time scales (Barreiro, 2010; Barreiro & Tippmann, 2008; Cai et al., 2020; Ropelewski & Halpert, 1987) and the Madden-Julian Oscillation (MJO) at intraseasonal (IS) time scales (Alvarez et al., 2016, 2017; Shimizu et al., 2017). These are the leading modes on their corresponding time scales and both are responsible for altering regional climate through, for example, modulating the frequency of occurrence of frontal systems, extratropical cyclones, or mesoscale convective systems.

Recently, it has been shown that different modes characterize IS variability depending on the season (Vera et al., 2018). The wet season (October-April) is characterized by the presence of a dipole-like spatial structure, which can be revealed by a principal component analysis of the rainfall field. This structure is known as the South American rainfall Dipole (SAD) (Boers et al., 2014; Nogués-Paegle & Mo, 1997), with centers located at the South Atlantic Convergence Zone (SACZ) and over Southeastern South America (SESA). The dry season (May-September), on the other hand, exhibits a monopole behavior centered at SESA. In our work we will focus on the SAD during the summer season, as this is the rainy season over most of South America.

The SAD characterizes the IS variability of the South American Monsoon System (SAMS) (Barros et al., 2002; Vera et al., 2006) and has been mainly related to the activity of the MJO (Alvarez et al., 2016, 2017;

Vera et al., 2018). The MJO has a characteristic time scale of about 30–80 days and can impact South America through two mechanisms: (a) a tropical-tropical pathway involving changes in the divergent circulation as the MJO propagates eastward, and (b) a tropical-extratropical pathway taking place through the excitation and dispersion of Rossby waves from the Indo-Pacific to the Atlantic region (Alvarez et al., 2016; Barreiro et al., 2019; Carvalho et al., 2004; De Souza & Ambrizzi, 2006; Gelbrecht et al., 2018; Gonzalez & Vera, 2014; Paegle et al., 2000; Shimizu & Ambrizzi, 2016). In particular, when the SACZ center is strengthened and the SESA center is weakened, the SAD phase has been associated with Phase 8-1 of the MJO. Similarly, when the SACZ center is weakened and the SESA center is strengthened, the SAD phase has been associated with the Phase 3-4 of the MJO. Moreover, SAD phases have been related with extreme precipitation events and severe droughts across SA (Boers et al., 2013; Carvalho et al., 2002), which have severe socioeconomic impact in highly populated areas, such as São Paulo or Buenos Aires, and are yet to be predicted. Hence, being able to predict SAD's behavior at the IS time scales in order to develop early warnings for extreme rainfall events is highly important.

In this work, we reveal the existence of intraseasonal predictability windows in the Accumulated SAD (ASAD) index during the months of December to March. Our methodology is based on defining a quantile-state time series from the ASAD index and on using the lagged mutual information (MI) to quantify the average amount of information shared by present and future quantile states. Our results show that, from present quantile states, we can forecast at 5 to 15 and 60 to 70 days ahead—to the best of our knowledge, IS forecast at 60 to 70 days has never been achieved before. These two predictability windows emerge robustly, that is, insensitive to changes in our control parameters (accumulated window size and poles' size), and reliably, that is, statistically significant at a 99% significance level and consistent across quantile choices (either median, terciles, or quartiles). We also reveal a third robust IS window at approximately 45 days, which only emerges when using quartile-states. In summary, we develop the first IS forecast for the ASAD index based on an approach that can be also applied to find predictions of other stationary time series.

The paper is organized as follows: Section 2 describes the data and our methodology, section 3 shows the main results and analysis, and section 4 has the conclusions.

2. Methods and Data

2.1. Data Specifics and the Construction of the SAD Index

We consider precipitation data from the Tropical Rainfall Measuring Mission (TRMM). These data consist of a multisatellite observation net, created to study the rainfall field over the tropics and subtropics. Although the mission (launched in 1997) ended in 2015, the data production was continued through the TRMM Multisatellite Precipitation Analysis (TMPA) (Huffman et al., 2007). Here, we use daily precipitation from the TMPA 3B42v7, which runs from 1 January 1998 to 31 December 2019 over a $0.25° \times 0.25°$ spatial grid. We only consider the months that the SAMS is in its mature stage (Vera et al., 2006), namely, December-January-February-March (DJFM). Thus, we avoid dealing with the developing [vanishing] stages of the transition from dry to wet [wet to dry] months, which introduce biases in the analysis.

In order to define the poles of the South American Dipole (SAD) from the precipitation anomaly fields, we follow the locations found by Vera et al. (2018). We construct a time series for each pole by averaging the anomalies within rectangular boxes placed at these two locations. Once both space-averaged time series are defined, we subtract the daily climatology for each time stamp and standardize using the daily standard deviation, resulting in a standardized anomaly time series for each pole. We then define the SAD index by subtracting the southern pole anomaly to the northern one. We use three box sizes (left panel in Figure 1) to carry an analysis on the sensitivity of our results to the spatial size of the poles.

In order to filter variability of the SAD on short time scales, while maintaining the intraseasonal (IS) time scales, we construct an Accumulated SAD (ASAD) index. We do this by adding the SAD daily data within sliding windows of 5, 7, or 9 days (making 1 day sliding translations of these windows), where we denote the resultant ASAD indexes as *accum*5, *accum*7, or *accum*9, respectively. This smoothing leaves the underlying physics unchanged at the IS time scale, as we show by testing our results' sensitivity to these three time scales.

2.2. Definition of Quantile States and Their IS Forecasting

The ASAD indexes (*accum*5, *accum*7, or *accum*9) are still too complex and insufficiently long (~2,500 data points in 21 years) to make reliable predictions with sufficient statistics. In other words, a real-valued time

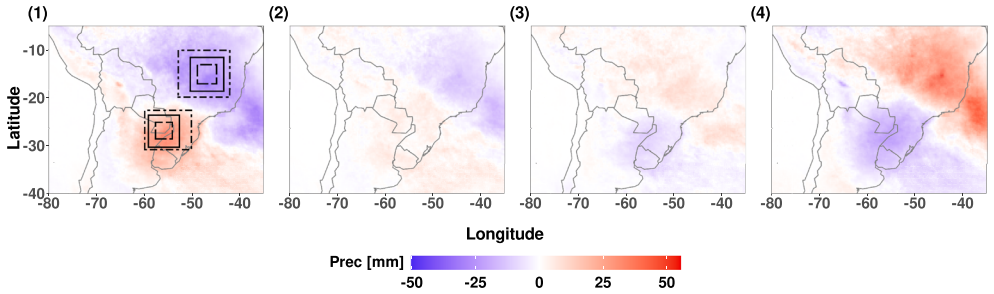

Figure 1. South American rainfall Dipole (SAD). Panel (1) shows the boxes used to construct the SAD index. From left to right, each panel shows the mean precipitation anomaly field of the accumulated SAD index (using 7 days accumulation windows) for the quartile-states defined over the dash-dotted-line box. States (1) and (4) [(2) and (3)] are extreme [neutral] SAD states.

series with 2,500 points is likely to have insufficient data for probability computations. Hence, we transform the ASAD index into a quantized time series, where each daily data corresponds to the ASAD's quantile-state at the time. We define a two-state time series from the distribution's median, three states from its terciles, and four states from its quartiles. For example, Figure 1 shows the mean precipitation anomaly fields for the region of interest corresponding to the quartile case. By doing this transformation, we can find statistically significant transition probabilities between the quantile states; therefore, we can make reliable forecasts. Also, we consider an IS forecast to be robust, only if it is insensitive to the choice of pole size (i.e., size of the boxes on the left panel of Figure 1) and sliding-window size that defines the ASAD index.

The transition probability of going from state x_i at time t to state x_j at time $t+\tau$ (τ being the time lag in days), with $i, j = 1, \ldots, N_Q$ (N_Q being the number of quantiles states, e.g., $N_Q = 4$ for quartiles), is

$$P\left(X_{t+\tau} = x_j | X_t = x_i\right) = P_{t,t+\tau}(j|i) \simeq P_\tau(j|i) \simeq \frac{N_\tau(j|i)}{\sum_{j=1}^{N_Q} N_\tau(j|i)}, \quad (1)$$

where X is the states' time series for one ASAD index, either *accum*5, *accum*7, or *accum*9. The first approximate equality ($P_{t,t+\tau} \simeq P_\tau$) is the assumption of an stationary X, implying that $P_{t,t+\tau}$ is invariant under time translations and independent of the starting time, t, for all i,j. We achieve this by choosing DJFM months, when the dipole is fully developed. Moreover, our daily standardization removes possible IS cycles that can break time translation invariance and our time series length (21 years) is insufficient to include climate change trends. The last approximate equality is the frequentist approach, where the transition probabilities are the frequency of appearance of state x_j at time $t+\tau$ when at time t the state was x_i, for all times t and fixed τ, that is, $N_\tau(j|i)$. We restrict $N_\tau(j|i)$ to consider only causal transitions, that is, transitions between states from the same DJFM period. Overall, $P_\tau(j|i)$ is our forecast.

In order to reliably select only the statistically significant forecasts, we construct a proportion test for Equation 1. The null hypothesis (NH) for it is that $X_t = x_i$ and $X_{t+\tau} = x_j$ are statistically independent, which implies that $P_\tau(j|i) = P(j)$ (i.e., the conditional probability is independent of the starting state and equal to the marginal probability of the ending state, $P(j)$). This NH is a Bernoulli process with two states: either $P(j)$ or $1 - P(j)$. We discard the NH at the 99% significance level only when $P_\tau(j|i)$ falls outside the z_{ij}-score's 99% central values. Specifically, the z_{ij}-score for each $P_\tau(j|i) = P(j)$ is

$$z_{ij} = \frac{P\left(X_{t+\tau} = x_j | X_t = x_i\right) - P\left(X = x_j\right)}{\sqrt{P\left(X = x_j\right)\left[1 - P\left(X = x_j\right)\right]/T}}, \quad (2)$$

where $P\left(X = x_j\right)$ is the marginal probability for the state x_j, with $i, j = 1, \ldots, N_Q$, and the denominator is the standard deviation for this Bernoulli process with T realizations. Given that z_{ij} distributions are asymptotically Gaussian, our 99% significance level is the Gaussian $z \approx 2.576$, which is our boundary to consider $P_\tau(j|i) \neq P(j)$.

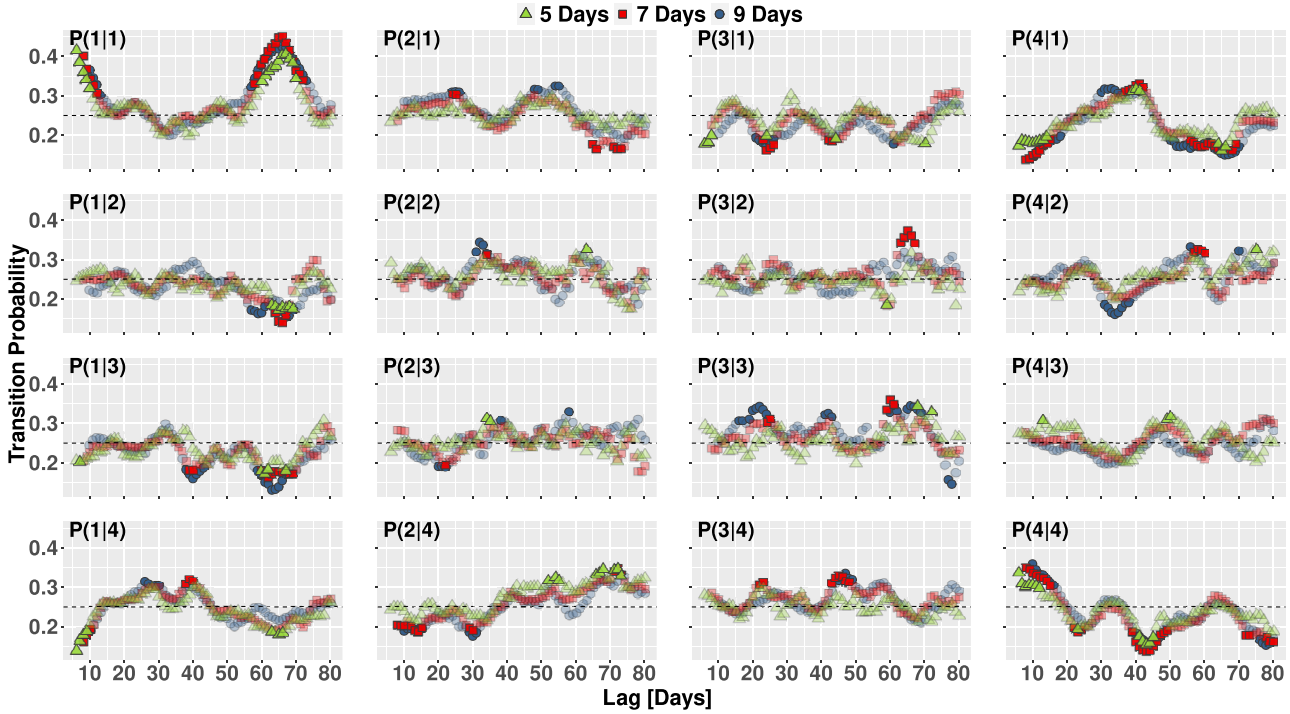

Figure 2. Transition probabilities, $P(j|i)$, between quartile states of the Accumulated South American rainfall Dipole (ASAD) index. $P(j|i)$ is shown as a function of the time difference, τ, between the starting quartile state i and the ending quartile state j ($i, j = 1, \ldots, 4$). Panels are organized in rows and columns according to the initial and final quartile-state, respectively. Window sizes of 5, 7, and 9 days used to construct the ASAD indexes, are shown by green triangles, red squares, and blue circles, respectively. Statistical dependence of state j to state i (at the 99% significance level) are signalled by solid symbols and statistical independence (i.e., null hypothesis) by transparent symbols.

3. Results and Analysis

3.1. Instraseasonal Predictability Windows

We begin by comparing the time series, *accum*, that result from using different pole sizes (see the three boxes in Figure 1), which we define to capture the South American Dipole (SAD) variability at different spatial scales. We quantify their similarities by the Pearson correlation coefficient (and the Spearman correlation; not shown), using a t test at a 99% significance level. This analysis holds significant correlation values (i.e., p values <0.01) for all *accum* indexes, ranging from 0.95 to 0.99—meaning that all pole sizes have similar time series. Hence, the SAD's behavior is captured robustly with either box. In what follows, we focus on the results from the largest (pole) box.

Without loss of generality, we show results for tercile and quartile states of the Accumulated SAD (ASAD) indexes. In particular, tercile statistics are commonly used in operational seasonal forecasting—defining positive, neutral, and negative dipole states. Quartile statistic's allow us to differentiate between extreme events—defining two extreme positive and negative states and two intermediate states—as well as to compare its results with the median case (see Supporting Information S1). Also, these quantile choices allows to have enough data for all transition probabilities, $P_\tau(j|i)$ [Equation 1].

In Figure 2 we show $P_\tau(j|i)$ for the quartile states ($N_Q = 4$ in Equation 1) of the ASAD indexes: *accum*5, *accum*7, and *accum*9. Marginal probabilities, $P(j)$, are signalled in all panels (as reference) by a horizontal, black, dashed line (which happens when the starting state does not influence the ending state). Panels are arranged from top to bottom (rows) according to the starting quartile state, x_i, at time t, and from left to right (columns) according to the ending quartile state, x_j, at time $t + \tau$.

The significant [insignificant] $P_\tau(j|i)$ values are shown with solid (transparent) symbols. We can distinguish the IS windows where a reliable forecast is possible, as the times τ where all three indexes have significant $P_\tau(j|i)$ values—which is discussed in section 3.2. Within these windows, we can forecast SAD quartile-states

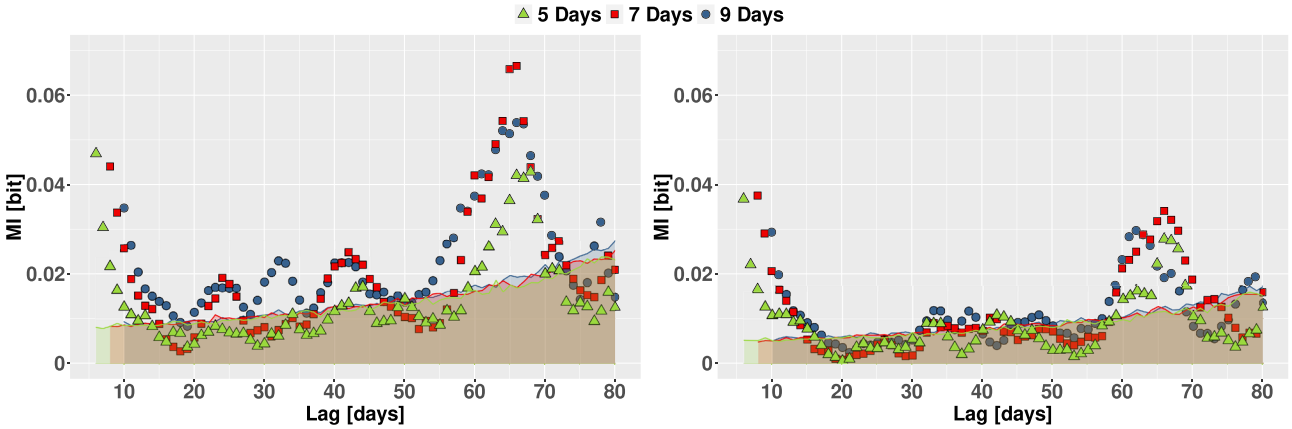

Figure 3. Lagged Mutual Information (MI) between quantile states of the accumulated precipitation anomalies of South American Dipole. Left (Right) panel shows the MI for the quartile states (tercile states) as a function of the time lag, τ, between starting and ending state. The symbols and colors are the same as in Figure 2. Shaded areas at the bottom correspond to the MI values of statistically independent surrogates at a 99% significance level.

transitions robustly and reliably; namely, the $P_\tau(j|i)$ values that are insensitive to parameter variations and are consistent across spatial and temporal scales.

Our main interest is to find intraseasonal (IS) predictability windows that are robust and reliable, disregarding the particular quartile-state (or tercile-state) transition that could be happening. In other words, we want to know when we can forecast the SAD states for any accumulated window size or quantile state. We do these by using the lagged Mutual Information (MI), $I(X_t;X_{t+\tau})$, which measures the average shared information between the states at time t and $t+\tau$ and is defined by (Cover & Thomas, 2012)

$$I(X_t;X_{t+\tau}) = \sum_{i=1}^{N_Q}\sum_{j=1}^{N_Q} P\left(X_t = x_i, X_{t+\tau} = x_j\right) \log_2\left[\frac{P\left(X_t = x_i, X_{t+\tau} = x_j\right)}{P\left(X_t = x_i\right) P\left(X_{t+\tau} = x_j\right)}\right], \quad (3)$$

$P\left(X_t = x_i, X_{t+\tau} = x_j\right) = P\left(X_t = x_i\right) P\left(X_{t+\tau} = x_j | X_t = x_i\right)$ being the joint probability of having state x_i at time t and state x_j at time $t+\tau$. We note that $I(X_t;X_{t+\tau}) = 0$ when $P\left(X_t = x_i, X_{t+\tau} = x_j\right) = P\left(X_t = x_i\right) P\left(X_{t+\tau} = x_j\right)$ for all i,j, corresponding to independent starting and ending states.

Figure 3 shows $I(X_t;X_{t+\tau})$ for all *accum* indexes, following the symbols and colors in Figure 2. Left (right) panel shows the resultant MI for the quartile (tercile) states. Confidence Intervals (CIs) at the 99% significance level are shown as transparent shaded areas for each *accum* index, which correspond to variables X_t and $X_{t+\tau}$ being statistically independent. These CIs are constructed by randomly resampling (with replacement) 10^3 times the original time series, where the objective is to construct a surrogate X_t and a $X_{t+\tau}$ time series. Also, for each *accum* index, the MI starts at different time lags, τ, because we discard the τ lags belonging to the accumulation window (namely, 5, 7, and 9 days), which naturally share information by construction.

From both panels in Figure 3, we can highlight two robust intraseasonal predictability windows where ASAD transitions can be predicted with 99% confidence; that is, values outside the shaded areas in either panel. Specifically, these windows—sharing significant information between the present and future ASAD states—are found at $\tau \approx 5$ to 15 days and at $\tau \approx 60$ to 70 days. We note that these windows also appear in our median analysis (see supporting information), making them a reliable forecast. As it is explained in section 3.2 by analyzing the specific transitions involved and taking into account previous works where possible mechanisms associated with the dipole phases were studied, we believe the first of these time windows can be associated to the mean persistence of the dipole extreme events, while the second one could be related to the MJO and to the presence of extratropical quasi-stationary Rossby waves.

We also note other predictability windows on the left panel of Figure 3, at IS scales of $\tau \approx 25$, $\approx$35, and $\approx$45 days. However, these windows are sensitive to the accumulated window size—with the exception of the quartile-state MI at $\tau \approx 45$ days. In particular, MI values for the *accum*5 index at $\tau \approx 25$ and $\approx$35 fall within the shaded areas, and all *accum* indexes fall within shaded areas for the terciles; as can be seen on the right panel of Figure 3. Hence, we deem these other predictability windows as unreliable indicators for

IS forecasting. In spite of this inconsistency in the forecasts, we obtain robust results for the quartile states at $\tau \approx 45$ days (namely, all ASAD indexes show a significant MI value for this window), which could also be related to the mechanisms already mentioned.

3.2. Forecasting States of the South American Rainfall Dipole

Having identified robust and reliable IS predictability windows from Figure 3, we can now critically analyze the state transitions in Figure 2, which are the reason for having these predictability windows. This analysis is particularly relevant when the final quartile state for which we can get information from the present is an extreme ASAD state. Physically, the smallest (largest) quartile corresponds to the southern (northern) pole having larger anomalies than the northern (southern) pole for about 5, 7, or 9 days (depending on the *accum* index). More importantly, from a practical point-of-view, identifying the relevant predictability windows allows to have concise forecasts for particular ASAD states. For example, by fixing τ (horizontal coordinate) and the starting quartile-state (row panels) in Figure 2, we can directly state the probability of transitioning to any of the four possible quartiles in τ days.

The first robust and reliable IS predictability window in Figure 3 happens at $\tau \approx 5$ to 15 days. As can be seen from the top—and bottom—corner panels in Figure 2, this window has significant MI values because of transitions happening between extreme quartile states, that is, States 1 and 4 (or tercile states; e.g., see Figure S1 in the supporting information). Particularly, the top (bottom) left and bottom (top) right panels show $P(1|1)$ [$P(1|4)$] and $P(4|4)$ [$P(4|1)$] having significantly higher [lower] probabilities than the marginal case, i.e., $P(1) = P(4) = 1/4$, respectively. On the other hand, all remaining transitions show an unconditional behavior, with transitions probability values similar to the marginal ones, for example, $P(2|2) \simeq P(2)$, $P(2|3) \simeq P(3)$, or $P(3|4) \simeq P(4)$. Hence, this predictability window has the following characteristics: likely persistence of extreme quartile states ($P(1|1)$ or $P(4|4) > 30\%$), unlikely transitioning between opposite extreme quartile states ($P(4|1)$ or $P(1|4) < 20\%$), and independent behavior for all remaining transitions.

From these characteristics, it seems clear that in this time window the system shows a persistence-like behavior. Once an extreme state pattern is established, it will persist for several days with the opposite state being unlikely to occur, as expected from the dipole character. This is consistent with previous works that studied the mean persistence of extreme events in the dipole phases. In Nogués-Paegle and Mo (1997), for example, the authors define extreme events of the dipole's phases through a principal component analysis over OLR data, finding mean duration times between 7 and 8 days. Taking into account that these are averages and that our indexes accumulate data for about a week, we can establish a connection between the first time window with the mean persistence of extreme dipole phases events.

The second robust and reliable IS predictability window in Figure 3 happens at $\tau \approx 60$ to 70 days. As can be seen from the left column panels in Figure 2, this window has significant MI values, mainly, because of transitions happening to the first quartile state, $P(1|j)$. Another contribution to this window's predictability comes from a decrease in the probability of transitioning from the extreme State 1 to the extreme State 4, that is, $P(4|1) < 20\%$ (top right panel in Figure 2). Secondary contributions appear inconsistently across other quartile states, such as $P(1|3)$ and $P(3|3)$, where transition probabilities are significant only for specific window-size accumulations.

Considering the first row in Figure 2, it seems that the second time window can be linked to a characteristic period of the dipole. That is, after ~65 days, the dipole is likely to be in State 1 and unlikely to be in the opposite state, 4. Vera et al. (2018) did a regression analysis between OLR anomaly data and the PC time series corresponding to the dipole's first EOF, finding that the SESA enhanced events—corresponding to our lower quartile state—present a characteristic period of about 50 days for DJF months. Even more, the maps show two mechanisms that are related to the dipole's behavior: (a) a tropical eastward propagating convection pattern resembling the average MJO behavior between Phases 1 and 5 (Alvarez et al., 2016; Wheeler & Hendon, 2004), and (b) an extratropical quasi-stationary wave train corresponding to a Rossby wave, which depending on the phase of the pressure center located at the tip of SA, favors one or the other dipole's phases. This last mechanism was also studied by Gelbrecht et al. (2018), where the authors found phase coherence between time indexes representing SESA and SACZ regions with a geopotential representing the Rossby wave train, with characteristic frequencies ranging from 1/50 to 1/10 days. Taking these studies into account, and particularly the frequencies found, we believe that these mechanisms are related to our second time window. Once again, the difference in the characteristic periods can be due to the accumulating process together with our quantization of the ASAD index.

To conclude our discussion, we illustrate how our approach allows to make forecasts. Lets consider first a $\tau =$ 10 days forecast. When the present ASAD index has a value in quartile 1, $P(1|1) \simeq 0.33$ and $P(4|1) \simeq 0.18$ after 10 days. Similarly, when the present ASAD index has a value in quartile 4, $P(4|4) \simeq 0.33$ and $P(1|4) \simeq 0.18$ after 10 days. However, the remaining transitions in Figure 2 from and to States 2 and 3 show inconclusive results. Similarly, we can make a forecast for $\tau = 45$ days. This particular forecast is only possible for quartile states, but it shows some insensitivity to the accumulation window and box size. For example, when the present ASAD index has a value in quartile 1, $P(4|1) \simeq 0.33$ after 45 days. Similarly, when the ASAD index has a value in quartile 4, $P(1|4) \simeq 0.18$ after 45 days. Overall, our methodology allows for the construction of transition probabilities, such as those in Figure 2, which allow to develop intraseasonal forecasts for the SAD states.

4. Conclusions

We employed a methodology based on statistical and information theory analysis, with the objective of studying intraseasonal (IS) predictability over the South American rainfall Dipole (SAD). By working with DJFM months, we are certain that the dipole system is in its mature stage and the time series have an stationary behavior. We defined the ASAD index—for 1 day sliding windows of accumulated rainfall anomalies of 5, 7, and 9 days—and introduced a finite set of states based on its quantiles (i.e., median, terciles, and quartiles). By doing this, we reduced the complexity of the ASAD index and were able to study the possible transitions between initial and final states (lagged by a time τ) with sufficient statistics.

By computing the lagged mutual information, we found that there are two IS time windows where the initial and final states share significant information (at a 99% significance level). Both of them were found robustly and reliably by taking into account the SAD index space variability (i.e., poles' sizes), the accumulation window for the ASAD index construction, and the quantile states considered.

The first time window is found from $\tau \approx 5$ to 15 days. We interpret this window as a persistence-like behavior, which extends beyond the synoptic time scale. The predictable states in this time window are the extreme ones (both for terciles and quartiles), which can be associated with the dipole phases. Hence, the persistence behavior could be interpreted as a mean-time duration of the dipole phases, which can be related to previous results where characteristic times between 7 and 8 days were associated to the dipole's extreme events. The second time window goes from $\tau \approx 60$ to 70 days. This result is consistent with the impact of the Madden-Julian Oscillation (MJO) on the intraseasonal time scales variability of the SAD and also with the presence of quasi-stationary extratropical Rossby waves and its influence on the dipole's phases.

Finally, we remark that by critically analyzing the specific transitions involved in each time window, we can forecast future states of the SAD by operationally observing the present states of the system for about 5 to 9 days. This allows, for the first time, to develop a quantile-based operational forecast system at IS time scales of the extreme phases of the main mode of rainfall variability in South America. In particular, we highlight the emergence of the 60 to 70 days predictability window, which appears independently of the box size that defines the poles, the accumulation window, or the quantile-states used to reduce the complexity in the index time series.

Data Availability Statement

The data used in this work are available from TRMM (TMPA) products (https://doi.org/10.5067/TRMM/TMPA/DAY/7).

Acknowledgments
All authors acknowledge PEDECIBA, Uruguay. N. D. acknowledges Comisión Académica de Posgrado (CAP), Uruguay. N. R. acknowledges the Comisión Sectorial de Investigación Científica (CSIC), Uruguay, group grant "CSIC2018-FID13-grupo ID 722."

References

Alvarez, M. S., Vera, C. S., & Kiladis, G. N. (2017). MJO modulating the activity of the leading mode of intraseasonal variability in South America. *Atmosphere*, *8*(12), 232.

Alvarez, M. S., Vera, C. S., Kiladis, G. N., & Liebmann, B. (2016). Influence of the Madden-Julian oscillation on precipitation and surface air temperature in South America. *Climate Dynamics*, *46*(1–2), 245–262.

Barreiro, M. (2010). Influence of ENSO and the South Atlantic ocean on climate predictability over southeastern South America. *Climate dynamics*, *35*(7–8), 1493–1508.

Barreiro, M., Sitz, L., de Mello, S., Franco, R. F., Renom, M., & Farneti, R. (2019). Modelling the role of Atlantic air–sea interaction in the impact of Madden–Julian oscillation on South American climate. *International Journal of Climatology*, *39*(2), 1104–1116.

Barreiro, M., & Tippmann, A. (2008). Atlantic modulation of El Niño influence on summertime rainfall over southeastern South America. *Geophysical Research Letters*, *35*, L16704. https://doi.org/10.1029/2008GL035019

Barros, V., Doyle, M., González, M., Camilloni, I., Bejarán, R., & Caffera, R. M. (2002). Climate variability over subtropical South America and the South American monsoon: A review. *Meteorologica*, *27*(1), 33–57.

Boers, N., Bookhagen, B., Marwan, N., Kurths, J., & Marengo, J. (2013). Complex networks identify spatial patterns of extreme rainfall events of the South American monsoon system. *Geophysical Research Letters*, *40*, 4386–4392. https://doi.org/10.1002/grl.50681

Boers, N., Rheinwalt, A., Bookhagen, B., Barbosa, H. M. J., Marwan, N., Marengo, J., & Kurths, J. (2014). The South American rainfall dipole: A complex network analysis of extreme events. *Geophysical Research Letters*, *41*, 7397–7405. https://doi.org/10.1002/2014GL061829

Cai, W., McPhaden, M. J., Grimm, A. M., Rodrigues, R. R., Taschetto, A. S., Garreaud, R. D., et al. (2020). Climate impacts of the El Niño–Southern Oscillation on South America. *Nature Reviews Earth & Environment*, *1*(4), 215–231.

Carvalho, L. M. V., Jones, C., & Liebmann, B. (2002). Extreme precipitation events in southeastern South America and large-scale convective patterns in the South Atlantic convergence zone. *Journal of Climate*, *15*(17), 2377–2394.

Carvalho, L. M. V., Jones, C., & Liebmann, B. (2004). The South Atlantic convergence zone: Intensity, form, persistence, and relationships with intraseasonal to interannual activity and extreme rainfall. *Journal of Climate*, *17*(1), 88–108.

Cavalcanti, I. F. A., Ferrerira, N. J., Silva, M. G. A. J., & Dias, M. A. F. (2016). *Tempo e clima no Brasil*. São Paulo: Oficina de textos.

Cover, T. M., & Thomas, J. A. (2012). *Elements of information theory*. New York: John Wiley & Sons.

De Souza, E. B., & Ambrizzi, T. (2006). Modulation of the intraseasonal rainfall over tropical Brazil by the Madden–Julian oscillation. *International Journal of Climatology: A Journal of the Royal Meteorological Society*, *26*(13), 1759–1776.

Garreaud, R. D., & Aceituno, P. (2007). Atmospheric circulation over South America: Mean features and variability. *The physical geography of South America*. Oxford, England: Oxford University Press.

Gelbrecht, M., Boers, N., & Kurths, J. (2018). Phase coherence between precipitation in South America and Rossby waves. *Science Advances*, *4*(12), eaau3191.

Gonzalez, P. L. M., & Vera, C. S. (2014). Summer precipitation variability over South America on long and short intraseasonal timescales. *Climate dynamics*, *43*(7–8), 1993–2007.

Huffman, G., Adler, R., Bolvin, D., Gu, G., Nelkin, E., Bowman, K., et al. (2007). The TRMM multisatellite precipitation analysis (TMPA): Quasi-global, multiyear, combined-sensor precipitation estimates at fine scales. *Journal of Hydrometeorology*, *8*, 38–55.

Nogués-Paegle, J., & Mo, K. C. (1997). Alternating wet and dry conditions over South America during summer. *Monthly Weather Review*, *125*(2), 279–291.

Paegle, J. N., Byerle, L. A., & Mo, K. C. (2000). Intraseasonal modulation of South American summer precipitation. *Monthly Weather Review*, *128*(3), 837–850.

Ropelewski, C. F., & Halpert, M. S. (1987). Global and regional scale precipitation patterns associated with the El Niño/Southern Oscillation. *Monthly Weather Review*, *115*(8), 1606–1626.

Shimizu, M. H., & Ambrizzi, T. (2016). MJO influence on ENSO effects in precipitation and temperature over South America. *Theoretical and applied climatology*, *124*(1–2), 291–301.

Shimizu, M. H., Ambrizzi, T., & Liebmann, B. (2017). Extreme precipitation events and their relationship with ENSO and MJO phases over northern South America. *International Journal of Climatology*, *37*(6), 2977–2989.

Vera, C. S., Alvarez, M. S., Gonzalez, P. L. M., Liebmann, B., & Kiladis, G. N. (2018). Seasonal cycle of precipitation variability in South America on intraseasonal timescales. *Climate Dynamics*, *51*(5–6), 1991–2001.

Vera, C., Higgins, W., Amador, J., Ambrizzi, T., Garreaud, R., Gochis, D., et al. (2006). Toward a unified view of the American monsoon systems. *Journal of Climate*, *19*(20), 4977–5000.

Wheeler, M. C., & Hendon, H. H. (2004). An all-season real-time multivariate MJO index: Development of an index for monitoring and prediction. *Monthly Weather Review*, *132*(8), 1917–1932.